Water Supply

Water Supply Vol 23 No 2, 688 doi: 10.2166/ws.2023.002

Soil moisture monitoring by downscaling of remote sensing products using LST/VI space derived from MODIS products

Amin Rostami [a,*], Mahmoud Raeini-Sarjaz[b], Jafar Chabokpour[c] and Aaron Anil Chadee[d]

[a] Irrigation and Drainage Engineering, Department of Water Engineering, Sari Agricultural Sciences and Natural Resources University, Sari, Iran
[b] Department of Water Engineering, Sari Agricultural Sciences and Natural Resources University, Sari, Iran
[c] Hydraulic Structures, Civil Engineering Department, University of Maragheh, Maragheh, Iran
[d] Civil and Environmental Engineering, University of the West Indies, St. Augustine, Trinidad
*Corresponding author. E-mail: amin.rostami6@gmail.com

AR, 0000-0002-0939-8444

ABSTRACT

Soil moisture (SM) has an important role in the earth's water cycle and is a key variable in water resources management. Considering the critical state of water resources in the Urmia Lake basin, northwest Iran, this study examined the potential for utilizing a variety of remote sensing data and products, in conjunction with a promising downscaling method, to monitor soil moisture with a reasonable spatial and temporal resolution, as a novel and effective tool for agricultural and water resource management. Accordingly, remote sensing products of surface soil moisture were scaled to MODIS's image scale (~1 km) using the UCLA downscaling method and Temperature, Vegetation, Drought Index (TVDI) values obtained from the scattering space method. Results showed that the LPRM, ESA-CCI, and GLDAS downscaled images had the highest inverse correlation with the TVDI (best results) accordingly equal to −0.600, −0.787, and −0.630. Also, based on the evaluation of the obtained results with the ground stations data, the LPRM and the ESA-CCI downscaled images had the best statistical indices values accordingly in 2010 and 2014 that confirm the promising application of remote sensing soil moisture data (r_{LPRM} (2010) = 0.92, MAE_{LPRM} (2010) = 4.14%, $RMSE_{LPRM}$ (2010) = 6.39% and $r_{ESA-CCI}$ (2014) = 0.7, $MAE_{ESA-CCI}$ (2014) = 2.23%, $RMSE_{ESA-CCI}$ (2014) = 2.59%).

Key words: ESA-CCI, GLDAS, LPRM, MODIS, triangular space, TVDI

HIGHLIGHTS

- Soil moisture spatio-temporal monitoring was carried out as an important step in the path of sustainable development.
- The research conducted on the downscaling of soil moisture radar products using MODIS images alongside scattering space and UCLA methods proved their ability in various land uses.
- LPRM and ESA-CCI products were found to have the highest accuracy in monitoring soil moisture in the Urmia Lake basin.

GRAPHICAL ABSTRACT

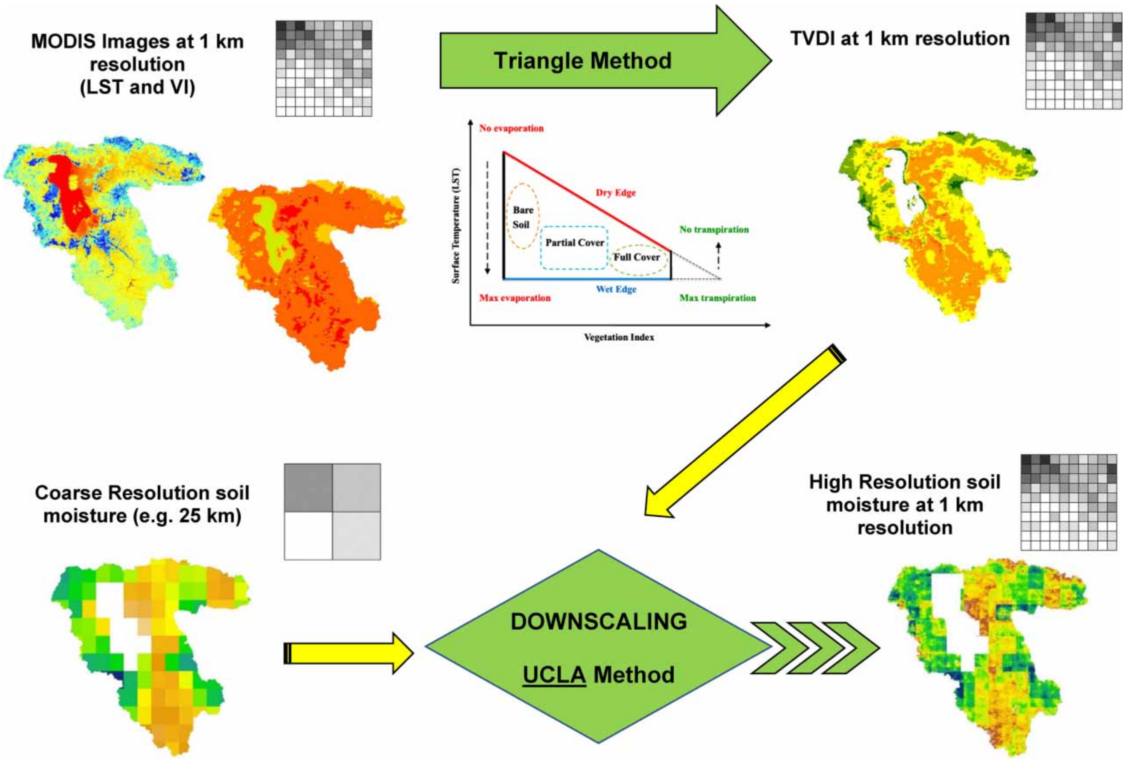

INTRODUCTION

Soil moisture (SM) is a major variable in the climate system, which controls the exchange of water, energy, and carbon flux between the earth's surface and the atmosphere (Ochsner *et al.* 2013). In global and regional water cycles, soil moisture is also one of the key parameters related to evapotranspiration, runoff occurrence, soil permeability, and groundwater recharge (Qiu *et al.* 2016). This 'soil moisture' is the water on the upper level of the soil profile and in the root zone or vadose area. Surface SM has received considerable attention for improving the predictive skills of runoff models that target flood risk prediction and/or water resource management (Entekhabi *et al.* 1999). For efficient irrigation management and planning, a consistent estimate of SM from agricultural fields is required (Glenn *et al.* 2011; Lorite *et al.* 2012; Srivastava *et al.* 2013b). Despite the importance of surface SM information, measured SM is present in only a limited number of field sites worldwide. Many factors affect the spatial distribution of SM, such as topographic changes, soil types, vegetation, climate, and aquifer water depth (Fernández-Prieto *et al.* 2012). On the other hand, because SM is highly variable in terms of space and time, *in situ* observations of SM, such as probe observations or gravimetric measurements, do not provide accurate and comprehensive information on the temporal and spatial distribution of SM and therefore are inappropriate for regional or global applications. Therefore, large-scale monitoring of SM can only rely on space-based remote sensing (Srivastava *et al.* 2013a, 2014). Although there are different types of remote sensing techniques for SM retrieval depending on the different electromagnetic spectra used, such as thermal, microwave, and visible infrared spectra, the accuracy of the prediction is ultimately determined by the soil moisture model.

The four dominant SM remote sensing methods based on spectrum characteristics are described below (Walker 1999; Vicente *et al.* 2004)

- Passive microwave (e.g., microwave spectrometers): calculation of SM by measuring brightness temperature (Tb), soil dielectric properties, and soil temperature.
- Active microwave (e.g., synthetic aperture radar – (SAR)): calculation of SM by estimating backscatter coefficient and dielectric properties.

- Visible: calculation of SM by determining soil albedo index of refraction.
- Thermal infrared: calculation of SM by measuring surface soil temperature.

The use of active microwave retrievals in measuring surface soil moisture is limited due to low temporal frequency and extreme sensitivity to vegetation and surface roughness (Walker *et al.* 2004). Passive microwave retrieval is the most effective method for soil moisture monitoring on a global scale due to the direct relationship between soil emissivity and soil moisture. These observations are also valid and applicable in all weather and vegetation conditions. Many microwave radiometers such as Special Sensor Microwave/Imager (SSM/I), Advanced Microwave Scanning Radiometer for EOS (AMSR-E), Soil Moisture and Ocean Salinity (SMOS) are used for soil moisture monitoring. However, the main disadvantage of passive microwave retrievals is their low spatial resolution, which is usually less than 25 km. Therefore, soil moisture retrieved with these observations is usually not sufficient for regional studies, and higher-resolution soil moisture monitoring is required (Kim & Hogue 2012). Methods have been developed to cover the reported limitations of microwave spectrum retrievals (low penetration in some weather and vegetation conditions, surface roughness effects, temporal frequency, and coarse spatial resolution) (Merlin *et al.* 2008; Kim & Hogue 2012). These methods generally fall into two categories: (1) Integration of passive and active microwave soil moisture retrievals to improve the coarse spatial resolution of data (Liu *et al.* 2012) and (2) integration of soil moisture data from microwave remote sensors and optical remote sensing soil moisture related products to achieve soil moisture data with relatively fine resolution (Chauhan *et al.* 2003; Piles *et al.* 2011; Choi & Hur 2012; Zhao & Li 2013). Data derived from optical remote sensors can provide detailed contextual information on the land surface. In this case, some studies have been made to improve the spatial and temporal signatures of microwave soil moisture by merging with visible and infrared (IR) products. These approaches have attracted significant attention since they do not require extensive ground-based data or model-based output and are relatively easy to implement.

Besides surface soil moisture data derived from microwave sensors, land surface parameters derived from multispectral optical remote sensing data have been used for estimating surface soil moisture since the early 1980s (Carlson *et al.* 1981, 1990, 1995; Patel *et al.* 2009; Rahimzadeh-Bajgiran *et al.* 2012; Leng *et al.* 2014). The normalized difference vegetation index (NDVI) is the most generally used vegetation index (VI) for investigating vegetation growth standing and is commonly declared as the greenness index, which indicates vegetation density and chlorophyll content of vegetation instead of the water condition of an area. Therefore, so as to observe water stress, there's a requirement for an additional sensitive indicator to NDVI. The values of land surface temperature (LST) measured high in dry conditions because of the dearth of soil moisture, and LST is used as a proxy for estimating the state of water stress. The NDVI and LST together will give crucial info on the status of vegetation and soil moisture (Gillies *et al.* 1997; Sandholt *et al.* 2002; Wan *et al.* 2004). Following this path, many studies have examined the appearance of a triangular or trapezoidal shape when drawing VI against LST (Carlson 2007). The appearance of the LST/VI triangular space is due to the low variations of LST over vegetated areas, and the high variations of LST in bare land areas (Sandholt *et al.* 2002). The focus of these studies is to analyze the biophysical characteristics enclosed in the LST/VI scatter space and to establish a relationship between these biophysical characteristics and the estimation of surface soil moisture (Carlson *et al.* 1990; Gillies *et al.* 1997; Petropoulos *et al.* 2009). Combining microwave retrievals and optical spectrum products of soil moisture is the most generally used technique for downscaling the coarse spatial resolution of soil moisture data retrieved from microwave observations. The LST/VI triangle space based models are the earliest and most commonly used methods. Based on the characteristics of the LST/VI feature space, Chauhan *et al.* (2003) first integrated passive microwave observations of soil moisture and optical remote sensing products by using a downscaling factor created based on the relatively high spatial resolution optical remote sensing data to improve the spatial resolution of soil moisture data. The method was straightforward to be enforced and commonly used since then (Ray *et al.* 2010; Piles *et al.* 2011; Choi & Hur 2012). Merlin *et al.* (2009, 2010) developed a spatial downscaling method by employing a semi-empirical soil evaporative efficiency model and integrating microwave retrievals of soil moisture and optical spectrum products, and this model is biophysically more accurate than the methods based on the LST/VI triangle space. However, because it requires several field measured biophysical parameters, the Merlin method cannot be easily applied. Kim & Hogue (2012) developed the UCLA[1] method, which applied the soil wetness index (Jiang & Islam 2003) obtained from MODIS[2] images as the downscaling factor to achieve relatively fine resolution soil moisture data from the coarse resolution

[1] University of California, Los Angeles.

[2] Moderate Resolution Imaging Spectroradiometer.

microwave retrievals of soil moisture. This study approved that the UCLA method had similar results to the Merlin method on downscaling of the coarse spatial resolution surface soil moisture data.

Now, considering the very small number and dispersion of ground stations for measuring soil moisture in Iran and the importance of knowing the spatial and temporal distribution of soil moisture in water resources and agriculture studies, this study aims to estimate the soil surface moisture using remote sensing data in Urmia Lake basin. For this purpose, the data of visible, near-infrared and thermal bands of MODIS sensor will be used. Radar data from AMSR-E, AMSR2[3], and ESA-CCI[4] satellites and LPRM[5] and GLDAS[6] models will be compared using the ground-based soil moisture data available in the study area. The results of this study can be applied as a practical method for researchers in other basins and also as an effective tool for policy makers and decision makers in the water resources and agriculture sector within the basin.

MATERIALS AND METHODS

The study area

The Urmia Lake basin is one of six major basins of Iran with an area of 51,876 km^2 between the orbits 40°35′ to 29°38′ north and east of the meridian of 13°44′ to 53°47′ located in the northwest of Iran. Figure 1 shows the geographical location and the land use map of the Urmia Lake basin. The Urmia Lake basin is located in the provinces of East and West Azerbaijan and Kurdistan. Its western border is the border heights of Iran and Turkey. The average annual rainfall varies from 350 to 600 mm and its predominant regime is the Mediterranean with little summer rainfall. Sabalan and Sahand mountains with a height of 4,811 and 3,707 m, respectively, are the highest points of this basin and Lake Urmia with an average height of 1,280 m is the deepest point of this basin. The main rivers of the basin are located in the southern half and the major ones are Aji Chai, Zarrinehrood, Siminehrood, Mahabadrood, Barandozchai, Zolachai and Nazlichai. Also, note that the rivers in the northern part have mainly small and low water basins.

Ground stations

Direct measurements of soil moisture at three ground stations in selected study areas were used to validate the remote sensing data and the estimates made in this study. Soil moisture in these stations is recorded at different soil depths and on weekly,

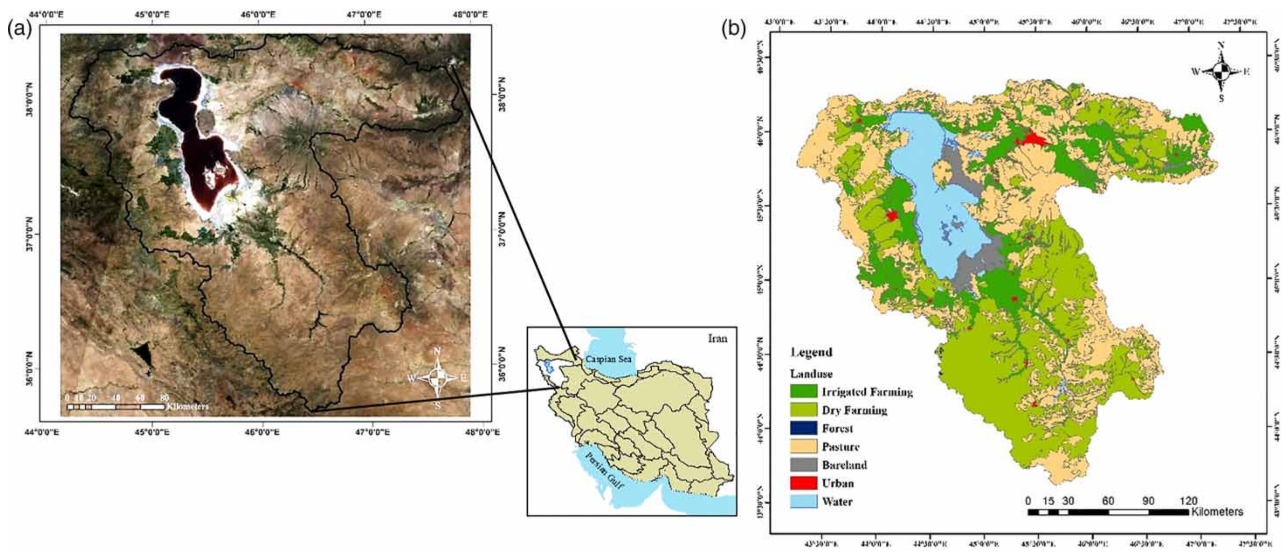

Figure 1 | (a) Location of the Urmia Lake basin in Iran (MOD09A1 image dated 4 July 2010) and (b) land use map of the Urmia Lake basin.

[3] Advanced Microwave Scanning Radiometer-2.

[4] European Space Agency – Climate Change Initiative.

[5] Land Parameter Retrieval Model.

[6] Global Land Data Assimilation System

daily, and hourly time scales. However, since the data and remote sensing methods used in this study estimate the soil moisture at a depth of 5 cm of the soil, only data recorded at a depth of 5 cm were used for validation. In statistical evaluations, the passing days of Terra satellite (MODIS sensor) were selected as the criterion and other observational data and remote sensing data were selected only for the selected 8-day time series from MODIS sensor images. The specifications of the selected stations and the statistical year of each station are given in Table 1.

Remote sensing data and models

The remote sensing data, its products and the earth data models used in this research are given in Table 2. Also in this table, the specifications related to the name of the satellite or radar, sensor and model used in the relevant product, the developer organization, as well as their spatial and temporal accuracy are given. The last column of this table lists the statistical year used for each product. The time series selected for all this data and products is the 8-day time series of MODIS sensor products (MOD09Q1 and MOD11A2) for both 2010 and 2014 from Julian day 65 (corresponding to March 6) to Julian day 265 (corresponding to September 22) and a total of 26 images were selected.

Remote sensing indices and methods

The NDVI

This index indicates the density of vegetation in the area and is calculated using bands 1 and 2 of MOD09Q1 images (Table 2) as follows (Du *et al.* 2017):

$$NDVI = \frac{\rho_2 - \rho_1}{\rho_2 + \rho_1}$$

Table 1 | Geographical characteristics of selected ground stations and statistical year used by each station in the study

Station	Latitude	Longitude	Altitude (m)	Year
Tabriz University Research Farm	38° 01′	46° 26′	1,670	210
Khosrowshah Meteorological Station	37° 58′	46° 02′	1,338	2014
Miandoab Meteorological Station	36° 58′	46° 03′	1,300	2014

Table 2 | Specifications of remote sensing and earth model data and products used in soil surface moisture remote sensing

Product	Satellite/Sensor/Radar/Model	Spectral band/ product	Spatial resolution (m)	Temporal resolution	Developer organization	Year
MOD09Q1	MODIS/Terra	Bands 1 and 2 of Modis	250	8 days	NASA	2010, 2014
MOD11A2	MODIS/Terra	LST	1,000	8 days	NASA	2010, 2014
CCI[a]	ERS-1/2, METOP[b], TMI, SMMR[c], AMSR-E, SSM/I, Windsat	Soil surface moisture	25,000	Daily	ESA-CCI	2010, 2014
LPRM	AMSR-E/Aqua	Soil surface moisture	25,000	Daily	NASA	2010
LPRM	AMSR2, GCOM/W1[d]	Soil surface moisture	10,000	Daily	NASA, JAXA	2014
AMSR-E	Aqua	Soil surface moisture	25,000	Daily	NASA	2010
GLDAS-Noah[e]	Ground and satellite data of various sources	Soil surface moisture	25,000	3 h	NASA	2014

[a]Climate Change Initiative.
[b]Meteorological Operational Satellite Program.
[c]Scanning Multi-channel Microwave Radiometer.
[d]Global Change Observation Mission – Water 1.
[e]Global Land Data Assimilation System/Noah.

In this equation, ρ_1 is the spectral reflectance of band 1 (bandwidth 620–670 nm) and ρ_2 is the spectral reflectance of band 2 (bandwidth 841–876 nm) of the mentioned images.

Land surface temperature

In this study, LST values are extracted from MOD11A2 images (Table 2) in °K.

LST/VI scatter plot diagram method (the triangular space method)

Numerous studies have been conducted to investigate the ability to use a combination of simultaneous remote sensing observations from the optical and thermal parts of the electromagnetic spectrum to extract surface soil moisture. Today, the ability to determine soil surface moisture in heterogeneous land surfaces using vegetation index values (VI) and surface temperature (LST) drawn in a two-dimensional space relative to each other (LST/VI scatter diagram) and mainly this space by a triangular amplitude is limited (provided that the full range of vegetation and soil moisture is shown in the data) (Carlson *et al.* 1995; Sandholt *et al.* 2002; Kato & Yamaguchi 2005; Wang *et al.* 2006; Hassan *et al.* 2007; Stisen *et al.* 2008; Patel *et al.* 2009; Shakya & Yamaguchi 2010; Petropoulos & Carlson 2011; Sobrino *et al.* 2012). Figure 2 shows the concept of the dependence of the ratio of soil temperature and vegetation on soil moisture. In the LST/VI scatter plot, the vertex of the triangle corresponds to an area with complete vegetation, while the base of the triangle corresponds to bare soil. The space between the vertex and the base of the triangle, which is most of the space of the triangle, is related to the surface of lands with variable vegetation. High-temperature pixels are related to dry soil conditions, while less scatter is observed in areas with wet soil conditions. LST/VI space depends on soil moisture based on the assumption that LST is more dispersed in an area with bare soil (especially on dry surfaces) than in an area with full vegetation (due to dispersion of soil moisture). Surface soil moisture changes from the left of the base to the right of the vertex in the triangle based on the values of temperature and VI in the transverse and longitudinal axes of the coordinates, respectively.

The Temperature, Vegetation, Drought Index

Various methods and indices have been developed to relate the characteristic LST/VI scatter space to surface soil moisture. One of these indicators is the Temperature, Vegetation, Drought Index (TVDI) which is defined as follows (Du *et al.* 2017):

$$TVDI = \frac{LST - LST_{min}}{LST_{max} - LST_{min}}$$

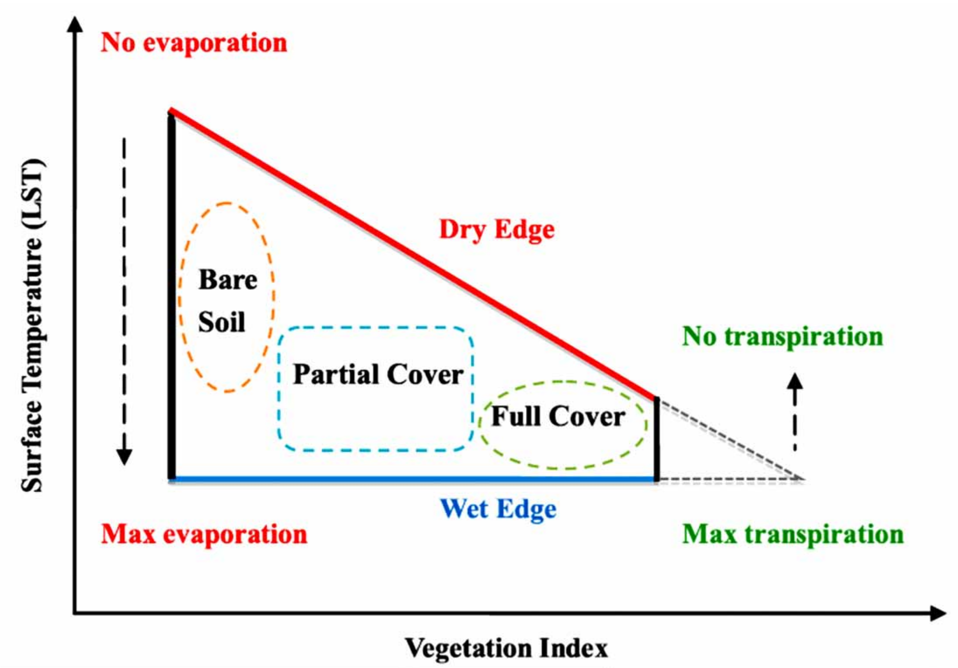

Figure 2 | Scatter space of land surface temperature in front of the VI (Peng *et al.* 2013).

In this equation, LST is the land surface temperature in °K and LST_{min} and LST_{max} values are calculated as follows (Du *et al.* 2017):

$$LST_{min} = a + b\ NDVI$$

$$LST_{max} = c + d\ NDVI$$

In which NDVI is the vegetation index (normalized vegetation difference index) and *a, b, c,* and *d* are the coefficients of the linear equations of the wet and dry edges of the triangular space, respectively.

Downscaling method

In this study, in order to estimate the soil surface moisture with spatial accuracy equal to the spatial accuracy of MODIS sensor (250 m), the values of soil surface moisture extracted from radar and model images (indicated in Table 2) with very low spatial accuracy (equal to 25 and 10 km) were used as real observational values and the TVDI index was used as a scale factor (which indicates the amount of soil surface moisture). The method used for downscaling is taken from the study of Kim & Hogue (2012) and is called the UCLA method. In the UCLA method, the amount of soil surface moisture with a spatial accuracy of 250 m MODIS is calculated as follows (Kim & Hogue 2012):

$$SM_{MODIS} = SM_{radar/model}\left(\frac{TVDI_{MODIS}}{\overline{TVDI}_{radar/model}}\right)$$

where SM_{MODIS} and $SM_{radar/model}$ are equal to the soil surface moisture with spatial accuracy of MODIS and the actual soil surface moisture extracted from the radar or model, respectively, and $TDVI_{MODIS}$ and $\overline{TVDI}_{radar/model}$ are equal to the TVDI index value with spatial accuracy of the MODIS and the average value of the TVDI per pixel of the corresponding radar or model, respectively.

Statistical evaluation indices

The statistical indices used to measure the error and accuracy of the estimates made in this study are mean bias error (MBE), mean absolute error (MAE), root mean square error ($RMSE$), concentrated root mean square error ($CRMSE$), model efficiency (EF), and correlation coefficient (R) are defined as follows (Cho *et al.* 2017; Cui *et al.* 2018):

$$MBE = \frac{1}{n}\sum_{t=1}^{n}(SM_{in-situ}(t) - SM_{RS}\ (t))$$

$$MAE = \frac{1}{n}\sum_{t=1}^{n}|SM_{in-situ}(t) - SM_{RS}\ (t)|$$

$$RMSE = \sqrt{\frac{1}{n}\sum_{t=1}^{n}(SM_{in-situ}(t) - SM_{RS}\ (t))^2}$$

$$CRMSE = \sqrt{\frac{1}{n}\sum_{t=1}^{n}[(SM_{in-situ}(t) - \overline{SM_{in-situ}(t)}) - (SM_{RS}\ (t) - \overline{SM_{RS}\ (t)})]^2}$$

$$EF = \frac{\sum_{t=1}^{n}(SM_{in-situ}(t) - \overline{SM_{in-situ}(t)})^2 - \sum_{t=1}^{n}(SM_{in-situ}(t) - SM_{RS}\ (t))^2}{\sum_{t=1}^{n}(SM_{in-situ}(t) - \overline{SM_{in-situ}(t)})^2}$$

$$R = \frac{\frac{1}{n}\sum_{t=1}^{n}[(SM_{in-situ}(t) - \overline{SM_{in-situ}(t)})\ (SM_{RS}\ (t) - \overline{SM_{RS}\ (t)})]}{\sigma_{SM_{in-situ}(t)}\ \sigma_{SM_{RS}(t)}}$$

In these equations, $SM_{in-situ}(t)$ and $SM_{RS}\ (t)$ were equal to the observed value (from ground stations) and the estimated value (from remote sensing data) for soil surface moisture, respectively, and the symbols^{-} and σ represent the mean value and the standard deviation of the corresponding values, respectively. The statistical indices of *MAE, RMSE, CRMSE* (to avoid possible biases) and model efficiency are used to measure the difference between the estimated and observational data series. The *MBE* index shows the average estimation tendency to overestimate or underestimate the observed values. A bias value of zero indicates that the estimation was able to predict the observed values well. Positive and negative values also indicate overestimation and underestimation of the estimation method, respectively. The correlation coefficient is also used to measure the relationship between two data sets.

RESULTS AND DISCUSSION

LST and NDVI

Figures 3 and 4 show some examples of spatial distribution maps of LST and vegetation index (NDVI). In the maps of June 26, which corresponds to the middle of the growing season, the distribution of agricultural plains with the high NDVI values (yellow and green areas in the NDVI maps) and the low LST values (yellow and orange areas in the LST maps). Of course, it should be noted that on this date, some highland and mountainous areas have similar characteristics due to relatively dense vegetation and low LST. In the NDVI map of September 6, the vegetation of these mountainous areas has also decreased and the green and yellow areas are only agricultural plains. However, the LST is still low in the highlands and is similar to agricultural plains.

Figures 5 and 6 show the temporal changes of the NDVI index and LST for 2010 and 2014 by land use classes. In the LST diagram, the curve for water bodies with the least change is the smoothest curve, and the curves for barren lands and forests have the highest changes. Also in this diagram, the lowest temperature is for water bodies and forests and the highest temperature is for barren lands and rainfed agricultural lands. Irrigated agricultural lands are also almost in the middle of this

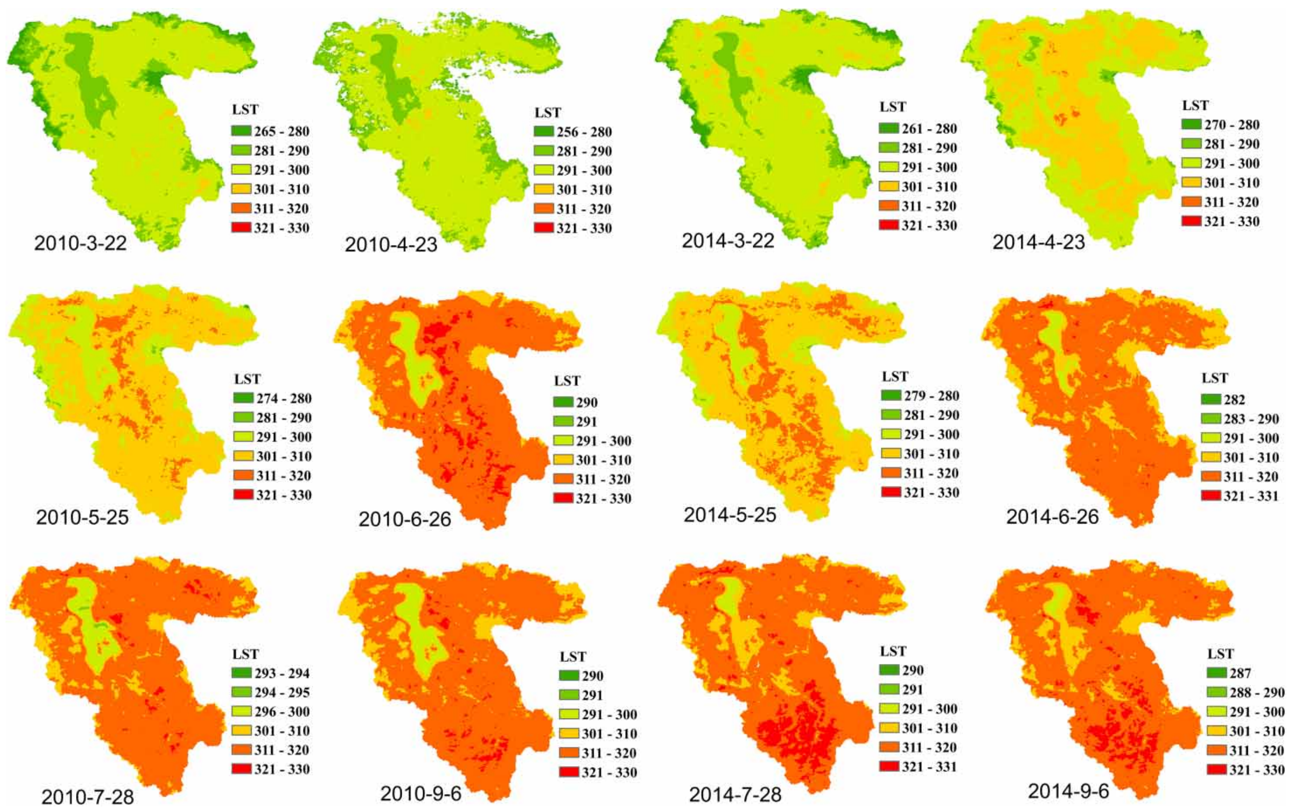

Figure 3 | Spatial distribution maps of land surface temperature. Please refer to the online version of this paper to see this figure in colour: http://dx.doi.org/10.2166/ws.2023.002.

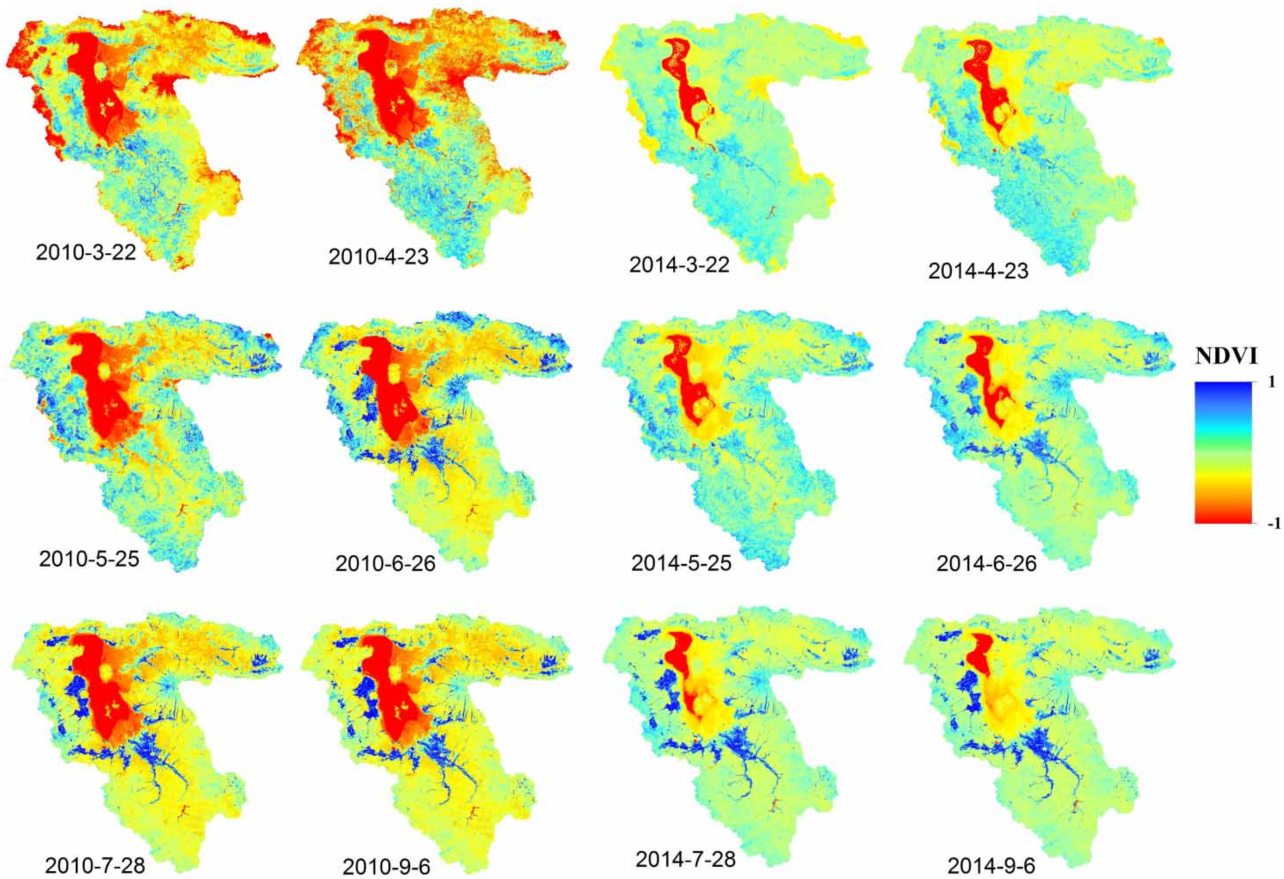

Figure 4 | Spatial distribution maps of the vegetation index (NDVI). Please refer to the online version of this paper to see this figure in colour: http://dx.doi.org/10.2166/ws.2023.002.

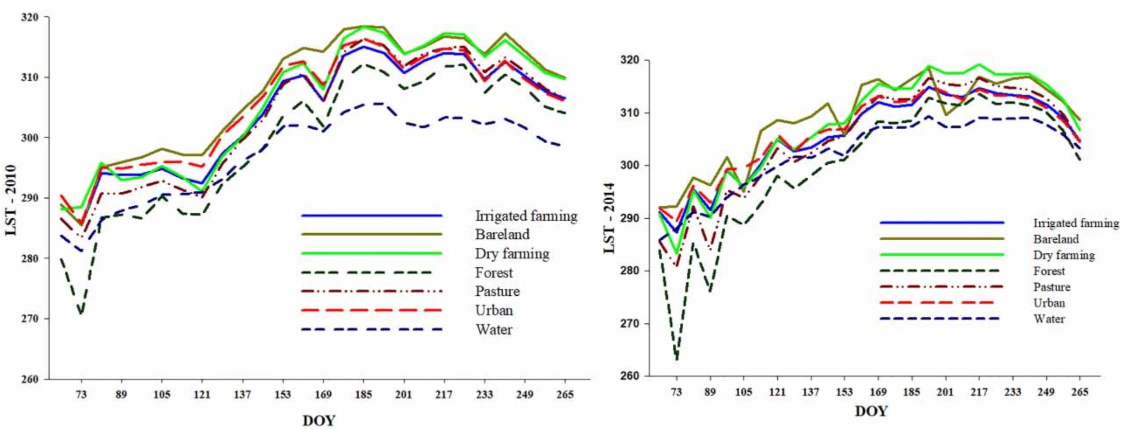

Figure 5 | Temporal changes of land surface temperature.

chart, the surface temperature has increased with a relatively uniform slope until the Julian day 177 in these lands, and then it has a constant trend and then decreased until the end of the season. In the NDVI diagram, the highest peak value is for forests on Julian day 137, followed by irrigated agriculture, rainfed agriculture and rangeland with the highest NDVI values. As expected, the lowest NDVI value is for barren lands. It is noteworthy that after Julian day 185, the amount of NDVI in forests decreases significantly. However, in irrigated agriculture, after a slight decrease for NDVI, which is due to the decrease in the

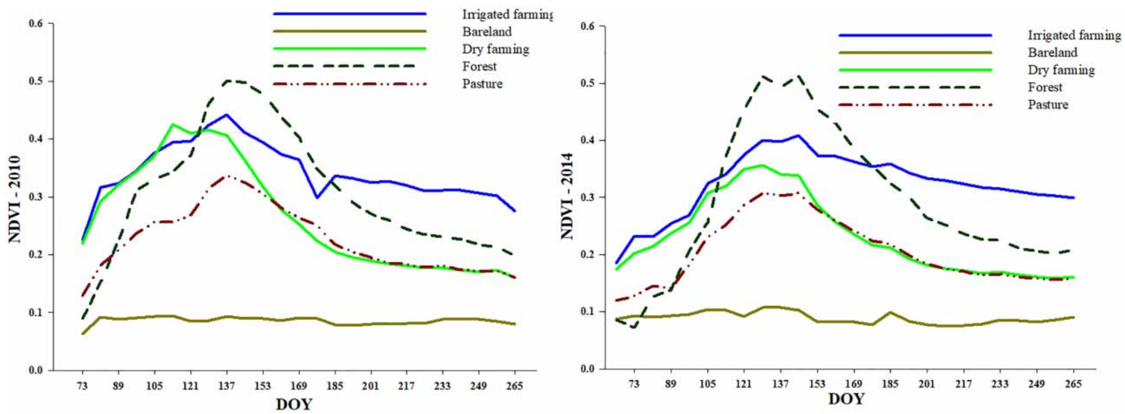

Figure 6 | Temporal changes of the NDVI.

greenness of the vegetation, the amount of NDVI remains almost constant until the end of the growing season, which is due to the presence of vegetation on the ground.

The TVDI

Figure 7 shows examples of LST-VI scatter plots for both study years. The date of the plots was selected to cover the entire study period at relatively regular intervals. The lines for the dry and the wet edges are also shown on these scatter plots. As can be seen, in most cases, the triangular (or trapezoidal) space is well formed, which indicates a wide range of soil moisture values in the study area. In many other studies, including Zhang *et al.* (2014); Carlson (2007); Murray & Verhoef (2007); Petropoulos *et al.* (2009), the formation of the trapezoidal space of the LST-VI scatter plot instead of the triangular space has been confirmed and reported.

Table 3 presents the coefficients of the linear equations of the dry and the wet edges as well as the correlation coefficient of each corresponding linear fit. As reported in Yang *et al.* (2008), the temporal variations of these coefficients do not have a specific order. In most cases, however, the slopes of the dry and wet edges have a similar trend, indicating that this scattering space will always be triangular or trapezoidal. In most cases, the value of the correlation coefficient is close to 0.9, which indicates the high accuracy of linear fitting of dry and wet edges.

According to the computational relations of TVDI index presented in the Materials and Methods section and by calculating the linear equations of dry and wet edges in LST-VI scattering space, spatial distribution maps of the temperature-vegetation-dryness index (TVDI) were obtained. Figure 8 shows the selected dates for both 2010 and 2014. All of these maps have been classified based on what was mentioned in Materials and Methods section in order to evaluate and compare them with each other. As can be seen, in 2014 the amount of land with severe and moderate drought is much higher than in 2010, which indicates the occurrence of drought in 2014. Similar results have been reported in the study of Rostami *et al.* (2017),

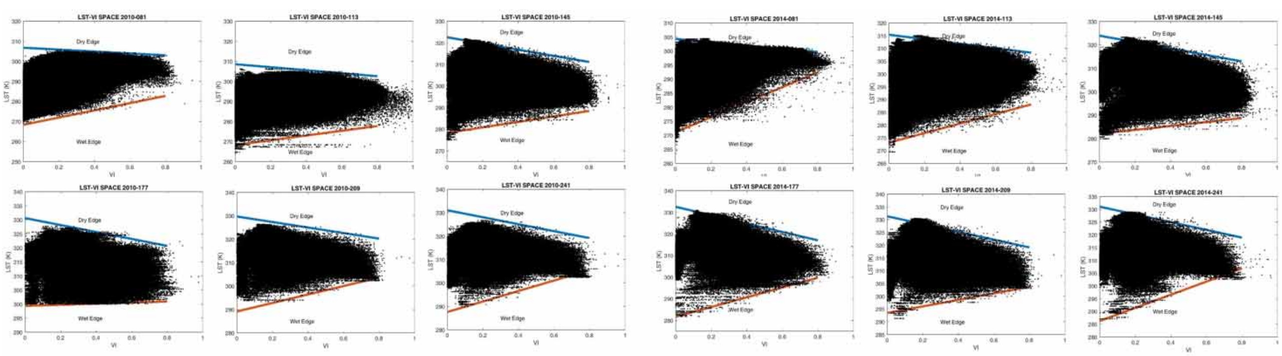

Figure 7 | LST-VI scatter plot diagrams on selected dates from 2010 to 2014.

Table 3 | Values of dry edge (a1, a2) and wet edge (b1, b2) equations in the studied days of 2010 and 2014

	a1		a2		b1		b2		R^2 (dry edge)		R^2 (wet edge)	
Julian Day	2010	2014	2010	2014	2010	2014	2010	2014	2010	2014	2010	2014
073	−6.18	−4.85	303.04	298.83	19.73	22.96	263.08	266.93	0.87	0.71	0.86	0.73
081	−4.72	−5.77	306.83	304.36	17.99	26.67	268.43	271.11	0.84	0.82	0.86	0.85
089	−8.67	−6.34	305.38	304.64	18.86	27.60	268.98	267.45	0.85	0.53	0.88	0.86
097	−10.92	−9.97	311.01	311.64	18.80	23.53	268.23	274.24	0.91	0.76	0.88	0.85
105	−10.96	−12.21	313.48	312.73	21.62	25.52	270.54	269.44	0.67	0.91	0.79	0.88
113	−7.50	−8.81	308.62	315.43	11.81	18.71	268.35	273.14	0.82	0.76	0.90	0.80
121	−11.77	−11.98	313.16	320.73	11.97	16.81	267.80	277.89	0.84	0.77	0.88	0.85
129	−15.81	−9.88	317.39	321.26	9.57	11.43	275.02	278.82	0.94	0.63	0.75	0.81
137	−12.23	−14.51	320.28	322.64	14.18	10.18	274.97	279.92	0.86	0.83	0.91	0.87
145	−14.32	−13.70	322.63	324.01	12.66	8.37	278.37	282.07	0.79	0.74	0.77	0.61
153	−14.40	−13.11	327.53	322.32	15.75	11.69	279.96	282.96	0.84	0.82	0.87	0.82
161	−16.49	−15.92	328.37	327.87	13.65	16.19	283.35	282.03	0.78	0.77	0.79	0.85
169	−13.53	−17.04	324.30	330.37	19.97	16.75	277.99	286.62	0.83	0.72	0.91	0.80
177	−12.37	−19.39	330.66	332.60	1.97	22.58	299.40	281.70	0.87	0.74	0.48	0.93
185	−13.33	−15.71	332.73	329.49	19.77	13.11	285.65	285.92	0.98	0.78	0.84	0.52
193	−18.04	−14.92	334.83	332.14	20.27	16.88	285.15	287.34	0.94	0.71	0.78	0.84
201	−20.79	−15.13	331.71	330.14	19.85	13.50	285.29	293.04	0.75	0.86	0.88	0.87
209	−11.80	−15.24	329.77	331.38	18.13	12.71	289.18	293.53	0.85	0.73	0.92	0.82
217	−16.94	−11.75	333.35	329.72	28.75	12.45	282.19	296.41	0.90	0.70	0.95	0.82
225	−17.57	−14.87	333.72	331.23	25.65	14.53	286.38	294.94	0.90	0.77	0.91	0.83
233	−22.70	−14.03	333.57	330.54	24.53	23.03	282.73	287.71	0.81	0.72	0.74	0.83
241	−14.87	−15.13	331.10	331.08	22.39	25.72	287.64	286.31	0.88	0.76	0.91	0.90
249	−12.43	−12.77	327.86	326.86	21.69	18.91	285.98	289.70	0.80	0.74	0.94	0.83
257	−16.25	−13.05	325.08	325.32	21.63	18.33	281.73	287.86	0.69	0.66	0.89	0.82
265	−18.53	−17.61	322.60	322.44	21.30	25.96	279.86	279.26	0.76	0.75	0.87	0.93

so that from the perspective of agricultural drought in 2014 in most areas of the Lake Urmia basin the moderate drought and in 2010 in most areas the normal situation is estimated. However, TVDI values in both 2010 and 2014 showed similar trends in spatial variation over the study period. Approaching the middle of the growing season (according to the middle dates), the amount of land with severe and moderate drought is reduced and the amount of wet and semi-wet land is increased, especially in agricultural and mountainous lands, although the rate of increase in 2010 was much higher. After that date, until the end of the growing season, the amount of the TVDI in agricultural lands as well as rangelands and barren lands will increase with decreasing greenness of vegetation and harvest of some agricultural products. In these maps, white areas are related to water bodies such as Lake Urmia and reservoirs of dams, in which the TVDI is not defined.

Figure 9 shows the diagram of temporal changes of the TVDI value in different land use classes of the Urmia Lake basin (except for water bodies) for both 2010 and 2014. Similarly, in both years, the forest class chart has the lowest TVDI values, indicating the high amount of soil moisture in these areas. Also, the highest values of the TVDI at the beginning of the study period are related to barren lands. In both years after Julian day 169, with the increase of rangeland vegetation in barelands, its chart is closer to the chart related to rainfed agricultural lands and even in 2014 is below dry farming graph. Graphs related to irrigated agricultural fields are slightly higher than pasture fields. From the middle of the growing season onwards with the growth of agricultural products and the increase in irrigation amount in irrigated fields, the amount of the TVDI in these fields decreases and is placed under the pasture graph. At the end of the study period, at the same time as harvesting crops and cutting off irrigation (and thus reducing soil moisture) in irrigated agricultural lands, the amount of the TVDI in these

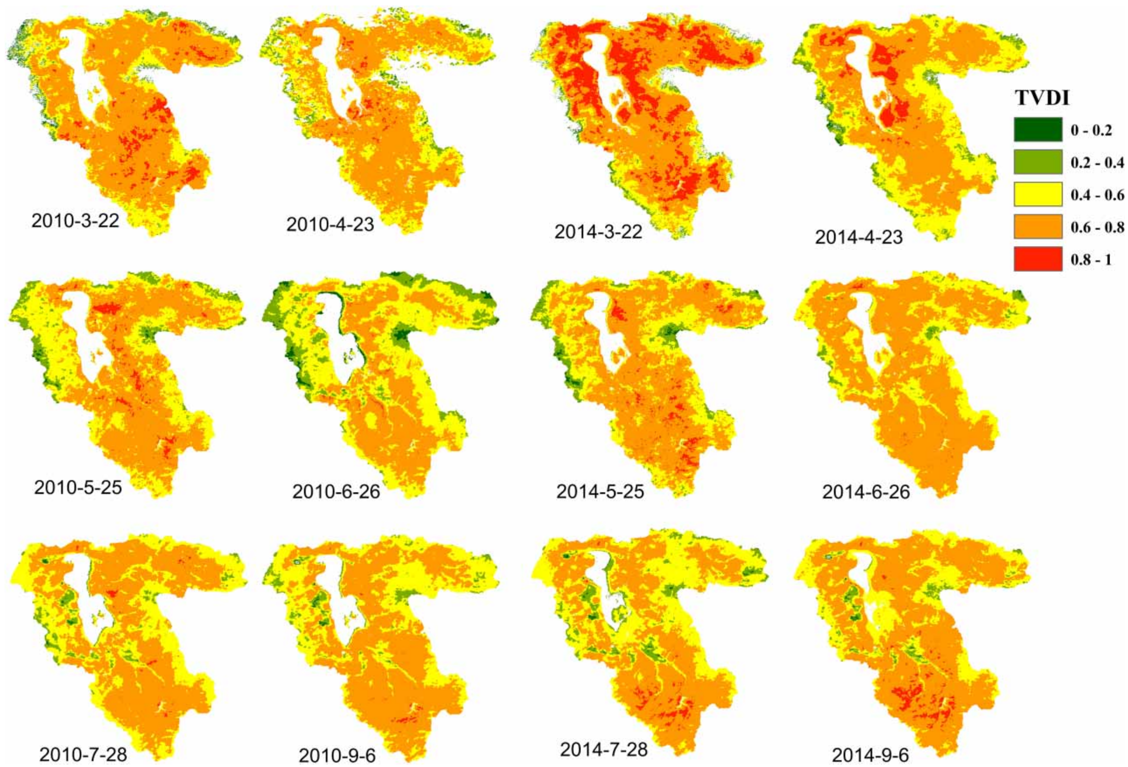

Figure 8 | Spatial distribution maps of the TVDI.

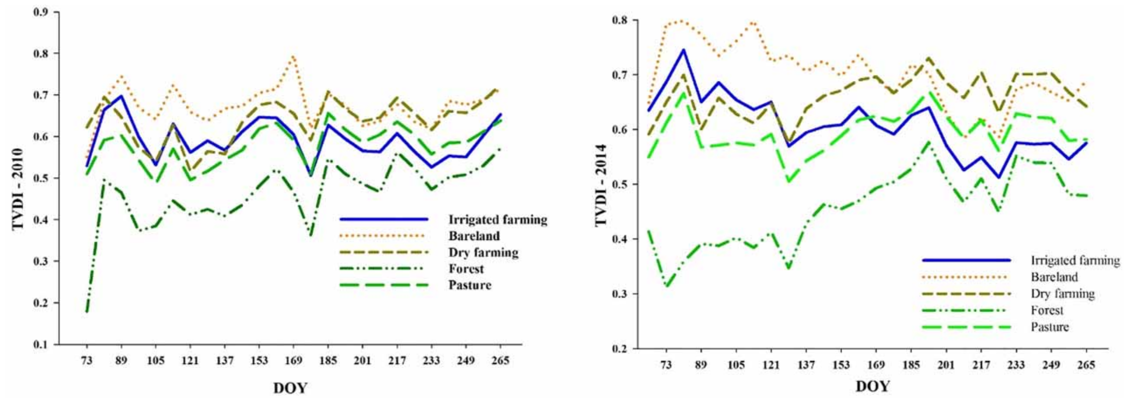

Figure 9 | Temporal changes of the TVDI.

fields is increasing and again approaches the TVDI diagram related to rangeland lands. As can be seen in these diagrams, the trend of temporal changes of TVDI index is different in each land use class, in forest lands, increasing trend, in barren lands, decreasing trend, and in agricultural lands (irrigated and rainfed) and rangeland, this diagram has both positive and negative slopes. This means that the amount of TVDI in the whole basin does not have a clear temporal changing pattern. Also, the fractures in these diagrams may be due to rainfall or irrigation in the relevant fields, which are similar to the results in the study of Du *et al.* (2017) and Yang *et al.* (2008).

Surface soil moisture

Spatial distribution maps of soil surface moisture obtained from radar images and various models using the triangular method and using the UCLA downscaling method for several samples from 2010 to 2014 are shown in Figure 10. Spatial accuracy in

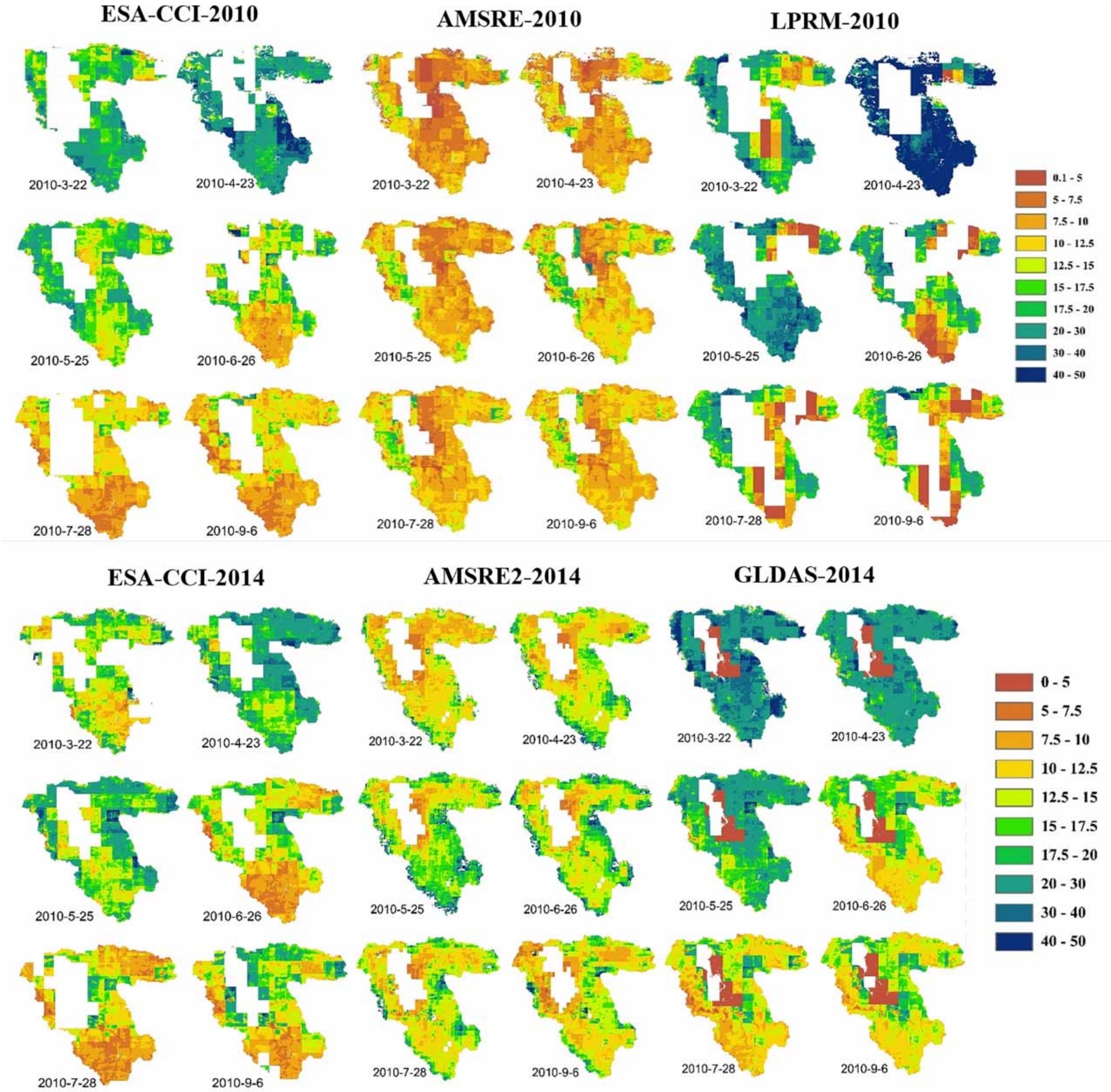

Figure 10 | Spatial distribution maps of soil surface moisture.

all these maps is equal to 1 km, and for the 8-day time series from Julius 65 to 265 in both 2010 and 2014 years, the results have been extracted. As shown in Figure 10, in 2010 the results of the ESA-CCI and LPRM images showed a similar trend in time and space. At the beginning of the season, the soil surface moisture in the whole basin and especially in the highlands and mountains was high due to snow cover and rainfall in late winter and early spring and gradually until late summer, the amount of soil surface moisture in these areas is reduced. In contrast, the amount of soil surface moisture in agricultural plains is higher than other areas of the basin in the middle and even late summer due to the presence of vegetation and irrigation of lands. The results of the LPRM model images have the highest number of uninformed pixels, which can limit the possibility of using the results in large basins, regardless of the accuracy of the estimates. The results of AMSRE radar only make sense in agricultural plains and pastures, but in other areas, including mountainous and highland areas and in the early period of the study, the surface soil moisture content has not been well estimated. The reason could be that the surface soil moisture product of AMSRE radar is related to vegetation moisture and is not very accurate in areas without vegetation and barelands. For 2014 (Figure 10) it can be seen that ESA-CCI and GLDAS images have estimated the trend of temporal and spatial changes in soil surface moisture in the same way as in 2010. Soil surface moisture in the whole basin has a relatively decreasing trend from early spring to late summer. Of course, agricultural and irrigated lands are an exception to this rule, and at the end of the study period, the amount of soil surface moisture in these areas is significantly higher than the adjacent lands and the areas of barren and mountainous lands. Since the images of the LPRM model for 2014 used AMSRE radar images, the trend and results of soil surface moisture in the whole basin have been estimated differently from the other two products and its results do not seem logical except in areas with vegetation (pastures and agricultural plains).

Comparison of downscaled images with radar and earth model images

Figure 11 shows some examples of different model images and radars for both 2010 and 2014 before and after the implementation of downscaling operations. The increase in the spatial accuracy and sharpness of the images in each particular case is quite evident in this figure, which is provided only for Julius 153 of both years to show the effect of downscaling in analyzing and evaluating the results of each model or radar. In so doing, the accuracy of images from schematic and spatial resolution at the global level (before downscaling) has become an acceptable accuracy in hydrological studies with spatial resolution of different land uses in the catchment area (after downscaling) while maintaining the overall spatial distribution pattern. Similar results and high accuracy of the UCLA downscaling method in combination with satellite optical and thermal images have been reported in previous studies including Kim & Hogue (2012) and Peng *et al.* (2015).

Statistical evaluations

Table 4(a) and (b) shows the correlation values of temperature variables and NDVI and TVDI with the results of soil surface moisture obtained from different data and models for both 2010 and 2014 years. In Table 4, the symbols * and ** at the top of each correlation number indicate the existence of a significant correlation at the level of 1 and 5% between the two comparable variables, respectively. Also, the sign of the positive and negative values of these numbers indicates the existence of direct and inverse correlations between the variables, respectively. As can be seen from the values in the table, in 2010, the soil surface moisture results of ESA-CCI and LPRM as expected are inversely and directly correlated with temperature and NDVI at 1%, respectively, and are inversely correlated with TVDI, for ESA-CCI it is significant at the level of 5% and for LPRM it is significant at the level of 1%. AMSRE radar results due to what has already been discussed about the nature of the captured data of this product, are only directly correlated with the LST variable at the 1% level. Also, as discussed in the previous section, the results of ESA-CCI and LPRM in 2010 have a direct correlation at the level of 1%, but compared to the AMSRE results, both products have an inverse correlation. In 2014, the results of ESA-CCI and GLDAS soil surface moisture variables with the LST variable are inversely correlated at the level of 1%, with the NDVI having a direct correlation

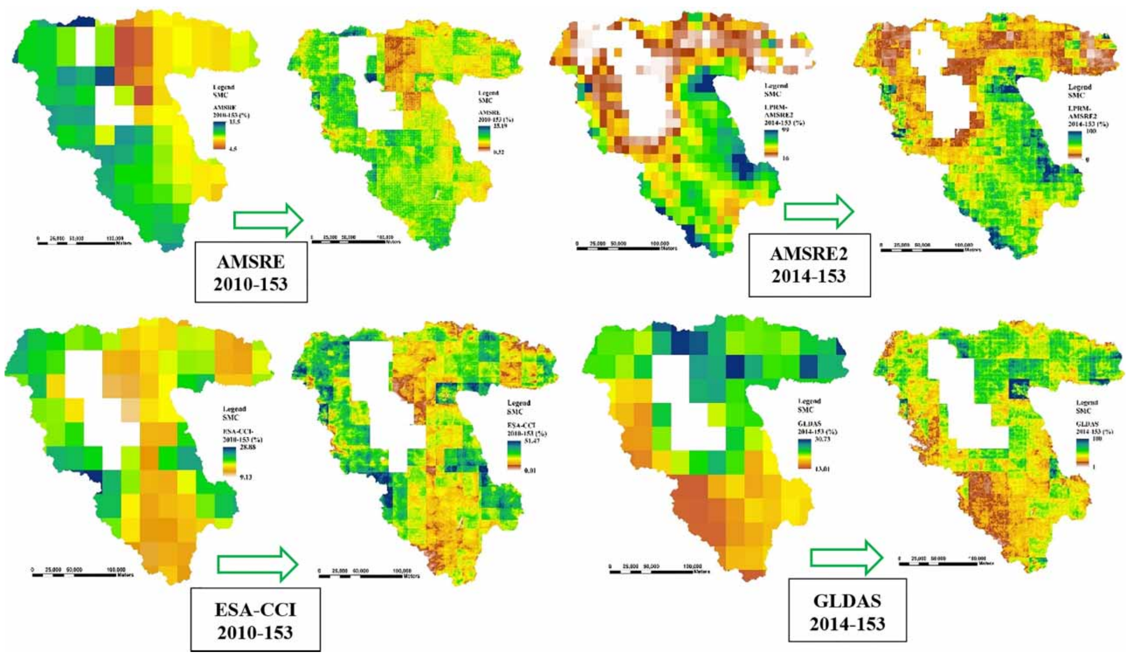

Figure 11 | Spatial distribution maps of soil surface moisture before and after downscaling on the Julian day 153 for the years 2010 and 2014 for some radar and model images.

Table 4 | Statistical correlation values of soil surface moisture obtained from different remote sensing data with NDVI, TVDI, and land surface temperature

a (2010)

	LST	NDVI	TVDI	AMSRE	LPRM	ESA-CCI
LST	1	−0.497**	0.440*	0.754**	−0.696**	−0.740**
NDVI	−0.497**	1	−0.379*	−0.282	0.712**	0.763**
TVDI	0.440*	−0.379*	1	0.236	−0.600**	−0.445*
AMSRE	0.754**	−0.282	0.236	1	−0.346*	−0.386*
LPRM	−0.696**	0.712**	−0.600**	−0.346*	1	0.772**
ESA-CCI	−0.740**	0.763**	−0.445*	−0.386*	0.772**	1

b (2014)

	LST	NDVI	TVDI	GLDAS	LPRM	ESA-CCI
LST	1	−0.548**	0.681**	−0.889**	0.781**	−0.872**
NDVI	−0.548**	1	−0.363*	0.392*	−0.650**	0.414*
TVDI	0.681**	−0.363*	1	−0.787**	0.428*	−0.630**
GLDAS	−0.889**	0.392*	−0.787**	1	−0.630**	0.802**
LPRM	0.781**	−0.650**	0.428*	−0.630**	1	−0.586**
ESA-CCI	−0.872**	0.414*	−0.630**	0.802**	−0.586**	1

at the level of 5% and with the TVDI are inversely correlated at the level of 1%. The results of LPRM model in 2014 have a direct and inverse correlation with the temperature variable and the NDVI at the level of 1%, respectively, and with the TVDI have a direct correlation at the level of 5%. These results are in accordance with what is discussed about the spatial distribution of soil surface moisture in the previous section. The results of ESA-CCI and GLDAS products in 2014 have a direct correlation at the level of 1%, but with the LPRM product (which results from AMSRE radar data) there is an inverse correlation.

In general, the results of this statistical evaluation confirm the reasonable and acceptable trend of LPRM and ESA-CCI products in 2010 and ESA-CCI and GLDAS products in 2014 in estimating temporal changes of soil surface moisture at the basin level.

Table 5 | The results of statistical indicators for soil surface moisture of remote sensing data with observational data in 2010 and 2014

	MBE (%)	*MAE* (%)	*RMSE* (%)	*EF*	*CRMSD*	*R*
Tabriz University Research Farm – 2010						
2010-AMSRE-SM	129.77	9.27	10.98	– 3.07	5.57	– 0.57*
2010-LPRM-SM	16.38	3.87	5.13	0.11	9.35	0.94**
2010-ESA-CCI-SM	43.18	4.14	6.39	– 0.38	8.77	0.92**
Khosrowshah Meteorological Station – 2014						
2014-GLDAS-SM	– 5.32	7.09	8.18	0.25	12.71	0.75**
2014-LPRM-SM	– 16.12	16.67	17.93	– 2.55	10.91	0.57*
2014-ESA-CCI-SM	– 0.50	7.04	7.95	0.35	10.51	0.70**
Miandoab Meteorological Station – 2014						
2014-GLDAS-SM	– 5.23	5.23	6.13	– 3.62	5.01	0.75**
2014-LPRM-SM	– 30.97	30.97	31.63	– 125.70	5.21	– 0.61*
2014-ESA-CCI-SM	– 1.28	2.23	2.59	0.15	3.11	0.62*

*Correlation is significant at the 0.05 level (1-tailed).

**Correlation is significant at the 0.01 level (1-tailed).

Table 5 shows the results of statistical evaluation of soil surface moisture values estimated from remote sensing data with observational data of Tabriz University station for 2010 and Khosroshah and Miandoab stations for 2014 in the form of introduced indicators. According to the values shown in the table, in 2010, the LPRM product with the lowest values of MBE, MAE, RMSE, CRMSD and the highest values of *R* and EF has the best results and AMSRE product shows the weakest results. ESA-CCI product ranks second in 2010 with weaker statistical index values than the LPRM product. In 2014, in both Khosroshah and Miandoab stations, ESA-CCI product shows the best results except *R*-correlation coefficient. For both stations, the LPRM product has the weakest results and GLDAS product with the highest correlation coefficient among the three products, but, with weaker results of other indicators compared to the ESA-CCI product, is in second place in 2014.

CONCLUSION

Given the importance of spatial and temporal monitoring of soil moisture at the basin scale, in this paper, using MODIS satellite images and LST-VI scattering space method, different remote sensing products of surface soil moisture with larger scales (10–25 km) were downscaled to the scale of MODIS's images (~1 km) by UCLA downscaling method. For this purpose, LST and NDVI variables were extracted using MODIS images. The study of spatial distribution maps of LST and NDVI showed the logical trend of spatial variation of these variables in the study area according to the land use map. Also, the study of temporal change graphs of LST and NDVI showed that estimating the time trend of variables in different land uses is reasonable and acceptable. Then the LST-VI scattering space was plotted for the studied time series and the equations of dry and wet edges were also extracted. Examination of these results showed that in all cases a triangular (or trapezoidal) space is formed, which indicates a wide range of soil moisture values in the study area. By estimating TVDI, studying the spatial distribution maps of the TVDI and its time change diagrams in different land uses showed that the trend of spatial and temporal changes of this index is logical and confirmed the accuracy of data and methods used in the study area. Finally, using the TVDI and the UCLA downscaling method, surface soil moisture maps were extracted at the MODIS images scale for various remote sensing products in the Urmia Lake basin. The study of these maps for 2010 and 2014 years as well as statistical evaluations on the results showed that in 2010 the LPRM product and in 2014 the ESA-CCI product had the best results in estimating surface soil moisture in the study area using the method used in this study.

Regarding the necessity of high spatial resolution in field-scale studies and, on the other hand, the relatively low spatial resolution of MODIS images and other remotely sensed soil moisture products applied in the present study, it is suggested that with the development of new remote sensing soil moisture products with higher spatial resolutions such as the Soil Moisture Active Passive (SMAP), similar studies can be performed using these products as well as optical satellite images with higher spatial resolutions, such as Landsat, SPOT, and ASTER images on smaller areas. Furthermore, to precisely assess the accuracy of products and methods used for remote sensing of surface soil moisture, similar studies could also be conducted in areas with more dense ground stations.

AUTHORS' CONTRIBUTIONS

A.R. and M.R.-S. studied and designed the concept; A.R. and J.C. collected data; A.R., M.R.-S., J.C., and A.A.C. performed the analyses and interpretation of results; A.R., J.C., and A.A.C prepared the draft manuscript. All authors reviewed the results and approved the final version of the manuscript.

DATA AVAILABILITY STATEMENT

The datasets generated during and/or analyzed during the current study is available from the corresponding author on reasonable request.

CONFLICT OF INTEREST

The authors declare there is no conflict.

REFERENCES

Carlson, T. N. 2007 An overview of the 'triangle method' for estimating surface evapotranspiration and soil moisture from satellite imagery. *Sensors* **7**, 1612–1629.

Carlson, T. N., Dodd, J. K., Benjamin, S. G. & Cooper, J. N. 1981 Satellite estimation of the surface energy balance, moisture availability and thermal inertia. *J. Appl. Meteorol. Climatol.* **20**, 67–87.

Carlson, T. N., Perry, E. M. & Schmugge, T. J. 1990 Remote estimation of soil moisture availability and fractional vegetation cover for agricultural fields. *Agric. Meteorol.* **52**, 45–69.

Carlson, T. N., Capehart, W. J. & Gillies, R. R. 1995 A new look at the simplified method for remote sensing of daily evapotranspiration. *Remote Sens. Environ.* **54**, 161–167.

Chauhan, N., Miller, S. & Ardanuy, P. 2003 Spaceborne soil moisture estimation at high resolution: a microwave-optical/IR synergistic approach. *Int. J. Remote Sens.* **24**, 4599–4622.

Cho, E., Su, C. H., Ryu, D., Kim, H. & Choi, M. 2017 Does AMSR2 produce better soil moisture retrievals than AMSR-E over Australia? *Remote Sens. Environ.* **188**, 95–105.

Choi, M. & Hur, Y. 2012 A microwave-optical/infrared disaggregation for improving spatial representation of soil moisture using AMSR-E and MODIS products. *Remote Sens. Environ.* **124**, 259–269.

Cui, C., Xu, J., Zeng, J., Chen, K.-S., Bai, X., Lu, H., Chen, Q. & Zhao, T. 2018 Soil moisture mapping from satellites: an intercomparison of SMAP, SMOS, FY3B, AMSR2, and ESA CCI over two dense network regions at different spatial scales. *Remote Sens.* **10** (1), 33.

Du, L., Song, N., Liu, K., Hou, J., Hu, Y., Zhu, Y., Wang, X., Wang, L. & Guo, Y. 2017 Comparison of two simulation methods of the temperature vegetation dryness index (TVDI) for drought monitoring in semi-arid regions of China. *Remote Sens.* **9**, 177.

Entekhabi, D., Asrar, G. R., Betts, A. K., Beven, K. J., Bras, R. L., Duffy, C. J., Dunne, T., Koster, R. D., Lettenmaier, D. P., McLaughlin, D. B., Shuttleworth, W. J., van Genuchten, M. T., Wei, M. Y. & Wood, E. F. 1999 An agenda for land surface hydrology research and a call for the second international hydrological decade. *Bull. Am. Meteorol. Soc.* **80**, 2043–2058.

Fernández-Prieto, D., van Oevelen, P. & Wagner, W. 2012 Advances in earth observation for water cycle science. *Hydrol. Earth Syst. Sci.* **16**, 543–549.

Gillies, R., Kustas, W. & Humes, K. 1997 A verification of the triangle method for obtaining surface soil water content and energy fluxes from remote measurements of the Normalized Difference Vegetation Index (NDVI) and surface e. *Int. J. Remote Sens.* **18**, 3145–3166.

Glenn, E. P., Neale, C. M. U., Hunsaker, D. J. & Nagler, P. L. 2011 Vegetation index-based crop coefficients to estimate evapotranspiration by remote sensing in agricultural and natural ecosystems. *Hydrol. Processes* **25**, 4050–4062.

Hassan, Q. K., Bourque, C. P. A., Meng, F. R. & Cox, R. M. 2007 A wetness index using terrain-corrected surface temperature and normalized difference vegetation index derived from standard MODIS products: an evaluation of its use in a humid forest-dominated region of eastern Canada. *Sensors* **7**, 2028–2048.

Jiang, L. & Islam, S. 2003 An intercomparison of regional latent heat flux estimation using remote sensing data. *Int. J. Remote Sens.* **24**, 2221–2236.

Kato, S. & Yamaguchi, Y. 2005 Analysis of urban heat island effect using ASTER and ETM + Data: separation of anthropogenic heat discharge and natural heat radiation from sensible heat flux. *Remote Sens. Environ.* **99**, 44–54.

Kim, J. & Hogue, T. S. 2012 Improving spatial soil moisture representation through integration of AMSR-E and MODIS products. *IEEE Trans. Geosci. Remote Sens.* **50**, 446–460.

Leng, P., Song, X., Li, Z. L., Ma, J., Zhou, F. & Li, S. 2014 Bare surface soil moisture retrieval from the synergistic use of optical and thermal infrared data. *Int. J. Remote Sens.* **35**, 988–1003.

Liu, Y. Y., Dorigo, W. A., Parinussa, R. D. J. R., Wagner, W., McCabe, M. F., Evans, J. P. & Van Dijk, A. I. J. M. 2012 Trend-preserving blending of passive and active microwave soil moisture retrievals. *Remote Sens. Environ.* **123**, 280–297.

Lorite, I. J., Garcı´a-Vila, M., Carmona, M. A., Santos, C. & Soriano, M. A. 2012 Assessment of the irrigation advisory services' recommendations and farmers' irrigation management: a case study in southern Spain. *Water Resour. Manage.* **26**, 2397–2419.

Merlin, O., Chehbouni, A., Walker, J. P., Panciera, R. & Kerr, Y. H. 2008 A simple method to disaggregate passive microwave-based soil moisture. *IEEE Trans. Geosci. Remote Sens.* **46**, 786–796.

Merlin, O., Al Bitar, A., Walker, J. P. & Kerr, Y. 2009 A sequential model for disaggregating near-surface soil moisture observations using multi-resolution thermal sensors. *Remote Sens. Environ.* **113**, 2275–2284.

Merlin, O., Duchemin, B., Hagolle, O., Jacob, F., Coudert, B., Chehbouni, G., Dedieu, G., Garatuza, J. & Kerr, Y. 2010 Disaggregation of MODIS surface temperature over an agricultural area using a time series of Formosat-2 images. *Remote Sens. Environ.* **114**, 2500–2512.

Murray, T. & Verhoef, A. 2007 Moving towards a more mechanistic approach in the determination of soil heat flux from remote measurements: I. A universal approach to calculate thermal inertia. *Agric. Meteorol.* **147**, 80–87.

Ochsner, T. E., Cosh, M. H., Cuenca, R. H., Dorigo, W. A., Draper, C. S., Hagimoto, Y., Kerr, Y. H., Larson, K. M., Njoku, E. G., Small, E. E. & Zreda, M. 2013 State of the art in large-scale soil moisture monitoring. *Soil Sci. Soc. Am. J.* **77**, 1888–1919.

Patel, N., Anapashsha, R., Kumar, S., Saha, S. & Dadhwal, V. 2009 Assessing potential of MODIS derived temperature/vegetation condition index (TVDI) to infer soil moisture status. *Int. J. Remote Sens.* **30**, 23–39.

Peng, J., Liu, Y., Zhao, X. & Loew, A. 2013 Estimation of evapotranspiration from TOA radiances in the Poyang Lake basin, China. *Hydrol. Earth Syst. Sci.* **17**, 1431–1444.

Peng, J., Niesel, J. & Loew, A. 2015 Evaluation of soil moisture downscaling using a simple thermal-based proxy–the REMEDHUS network (Spain) example. *Hydrol. Earth Syst. Sci.* **19**, 4765–4782.

Petropoulos, G. P. & Carlson, T. N., 2011 Retrievals of turbulent heat fluxes and soil moisture content by Remote Sensing. In: *Advances in Environmental Remote Sensing: Sensors, Algorithms, and Applications*, 1st edn (Qihao, W., ed.). CRC Press, Boca Raton, FL, USA, pp 469–501.

Petropoulos, G., Carlson, T., Wooster, M. & Islam, S. 2009 A review of Ts/VI remote sensing based methods for the retrieval of land surface energy fluxes and soil surface moisture. *Prog. Phys. Geogr.* **33**, 224–250.

Piles, M., Camps, A., Vall-Llossera, M., Corbella, I., Panciera, R., Rudiger, C., Kerr, Y. H. & Walker, J. 2011 Downscaling SMOS-derived soil moisture using MODIS visible/infrared data. *IEEE Trans. Geosci. Remote Sens.* **49**, 3156–3166.

Qiu, J., Gao, Q., Wang, S. & Su, Z. 2016 Comparison of temporal trends from multiple soil moisture data sets and precipitation: the implication of irrigation on regional soil moisture trend. *Int. J. Appl. Earth Obs. Geoinf.* **48**, 17–27.

Rahimzadeh-Bajgiran, P., Omasa, K. & Shimizu, Y. 2012 Comparative evaluation of the Vegetation Dryness Index (VDI), the Temperature Vegetation Dryness Index (TVDI) and the improved TVDI (iTVDI) for water stress detection in semi-arid regions of Iran. *ISPRS J. Photogramm. Remote Sens.* **68**, 1–12.

Ray, R. L., Jacobs, J. M. & Cosh, M. H. 2010 Landslide susceptibility mapping using downscaled AMSR-E soil moisture: a case study from Cleveland Corral, California, US. *Remote Sens. Environ.* **114**, 2624–2632.

Rostami, A., Bazzane, M. & Raeini, M. 2017 Spatial and temporal monitoring of agricultural drought using MODIS sensor images and remote sensing techniques (A case study: East Azerbaijan Province). *Water and Soil Science* **27** (1), 213–226.

Sandholt, I., Rasmussen, K. & Andersen, J. 2002 A simple interpretation of the surface temperature/vegetation index space for assessment of surface moisture status. *Remote Sens. Environ.* **79**, 213–224.

Shakya, N. & Yamaguchi, Y. 2010 Vegetation, water and thermal stress index for study of drought in Nepal and central northeastern India. *Int. J. Remote Sens.* **31**, 903–912.

Sobrino, J., Franch, B., Mattar, C., Jiménez-Muñoz, J. & Corbari, C. 2012 A method to estimate soil moisture from Airborne Hyperspectral Scanner (AHS) and ASTER data: application to SEN2FLEX and SEN3EXP campaigns. *Remote Sens. Environ.* **117**, 415–428.

Srivastava, P. K., Han, D., Ramirez, M. A. & Islam, T. 2013a Machine learning techniques for downscaling SMOS satellite soil moisture using MODIS land surface temperature for hydrological application. *Water Resour. Manage.* **27**, 3127–3144.

Srivastava, P. K., Han, D., Rico-Ramirez, M. A., Al-Shrafany, D. & Islam, T. 2013b Data fusion techniques for improving soil moisture deficit using SMOS satellite and WRF-NOAH land surface model. *Water Resour. Manage.* **27**, 5069–5087.

Srivastava, P. K., Han, D., Rico-Ramirez, M. A., O'Neill, P., Islam, T. & Gupta, M. 2014 Assessment of SMOS soil moisture retrieval parameters using tau-omega algorithms for soil moisture deficit estimation. *J. Hydrol.* **519**, 574–587.

Stisen, S., Sandholt, I., Nørgaard, A., Fensholt, R. & Jensen, K. H. 2008 Combining the triangle method with thermal inertia to estimate regional evapotranspiration – applied to MSG-SEVIRI data in the Senegal River basin. *Remote Sens. Environ.* **112**, 1242–1255.

Vicente, S., Pons, F. N. & Cuadrat, P. 2004 Mapping soil moisture in the central Ebro river valley (northeast Spain) with Landsat and NOAA satellite imagery: a comparison with meteorological data. *Int. J. Remote Sens.* **25**, 4325–4350.

Walker, J. P. 1999 *Estimating Soil Moisture Profile Dynamics From Near-Surface Soil Moisture Measurements and Standard Meteorological Data*. *Dissertation*, University of Newcastle, Newcastle, UK.

Walker, J. P., Houser, P. R. & Willgoose, G. R. 2004 Active microwave remote sending for soil moisture measurement: a field evaluation using ERS-2. *Hydrol. Processes* **18**, 1975–1997.

Wan, Z., Wang, P. & Li, X. 2004 Using MODIS land surface temperature and normalized difference vegetation index products for monitoring drought in the southern Great Plains, USA. *Int. J. Remote Sens.* **25**, 61–72.

Wang, K., Li, Z. & Cribb, M. 2006 Estimation of evaporative fraction from a combination of day and night land surface temperatures and NDVI: a new method to determine the Priestley–Taylor parameter. *Remote Sens. Environ.* **102**, 293–305.

Yang, X., Wu, J., Shi, P. & Yan, F. 2008 Modified triangle method to estimate soil moisture status with MODerate resolution Imaging Spectroradiometer (MODIS) products. *Proc. Int. Arch. Photogramm. Remote Sens. Spat. Inf. Sci.* **37**, 555–560.

Zhang, F., Zhang, L. W., Jing-Jing, S. & Huang, J. F. 2014 Soil moisture monitoring based on land surface temperature-vegetation index space derived from MODIS data. *Pedosphere* **24** (4), 450–460.

Zhao, W. & Li, A. 2013 A downscaling method for improving the spatial resolution of AMSR-E derived soil moisture product based on MSG-SEVIRI data. *Remote Sens.* **5**, 6790–6811.

First received 27 August 2022; accepted in revised form 23 December 2022. Available online 17 January 2023